Self-Interference Cancellation in Digital Sensing and Communication Arrays

Jan Adler
Wireless Connectivity & Sensing
Barkhausen Institut
Dresden, Germany
jan.adler@barkhauseninstitut.org

Maximilian Matthé
Connected Robotics Lab
Barkhausen Institut
Dresden, Germany
maximilian.matthe@barkhauseninstitut.org

***Abstract*—Self-interference is a key factor limiting the sensing performance of monostatic integrated sensing and communication systems. This paper presents a frequency-domain approach to estimating the self-interference characteristics of fully digital multi-antenna arrays and derives a precoding scheme for analog self-interference cancellation.**

I. Introduction

Integrated Sensing and Communications (ISAC) is quickly evolving to be one of the key features introduced with the 6-th generation standard of wireless networks [1]–[3]. It promises to enable sensing as an additional service offered by communication base stations, add sensing capabilities to internet-of-things devices and communication terminals, as well as merge sensing and communication features in automotive and robotic applications [4], [5]. Sensing and communications traditionally deploy different radio-frequency (RF) front-ends [6]. In monostatic configurations, where transmitters and receivers are co-located and simultaneously transmit and receive in identical time slots and frequency bands in an in-band full duplex fashion, one of the factors limiting the receive performance is self-interference resulting from the transmitted waveforms directly being picked up by receiving antennas and RF circuits [7]–[9]. Self-interference can be addressed at multiple points of the analog signal processing, for example by optimizing antenna arrays for minimal power leakage or adding cancellation circuits in between transmitting and receiving RF circuits. Fully digital antenna arrays, where each antenna element is connected to a dedicated RF chain and analog to digital converter (ADC) or digital to analog converter (DAC), offer the unique opportunity of directly optimizing the generated base-band waveforms for minimal self-interference by considering the unique frequency-selective characteristics in between each pair of transmit- and receive RF chains. Based on a detailed system model, derived in section II, this paper proposes a self-interference frequency-domain estimation algorithm in section III followed by a digital precoding approach in section IV. The proposed algorithms are finally validated by hardware measurements presented in section V.

This work was financed with tax revenue on the basis of the budget approved by the Saxon state parliament and the European Union's Horizon Europe SNS project INSTINCT (grant agreement no. 101139161).

II. System Model

The considered system consists of an arbitrary antenna array topology featuring M receive chains and N transmit chains, with each transmitting antenna being fed by a dedicated DAC and each receiving antenna feeding into a dedicated ADC, respectively. The system model is visualized in Figure 1. Within transmit chains, the DACs generate N complex base-band signals

$$\mathbf{x}(t) = \left[x^{(1)}(t), \dots, x^{(N)}(t)\right]^{\mathsf{T}} \in \mathbb{C}^N \tag{1}$$

propagating over RF front-ends into transmitting antenna elements. Inversely, within receive chains,

$$\mathbf{y}(t) = \left[y^{(1)}(t), \dots, y^{(M)}(t)\right]^{\mathsf{T}} \in \mathbb{C}^M \tag{2}$$

denotes the M base-band signals being sampled by receiving ADCs after impinging onto their respective antenna elements and subsequent analog processing by interconnecting RF front-ends. The m-th received base-band signal

$$y^{(m)}(t) = y^{(m)}_{\mathrm{Int}}(t) + y^{(m)}_{\mathrm{Rad}}(t) + n^{(m)}(t) \tag{3}$$

is assumed to be a superposition of self-interference $y^{(m)}_{\mathrm{Int}}(t)$ leaking from transmit chains into the receive chains, environmental scattering from illuminated radar targets in the antenna array's far-field $y^{(m)}_{\mathrm{Rad}}(t)$, and circularly invariant additive white Gaussian noise

$$n^{(m)}(t) \sim \mathcal{CN}(0, \sigma^2) \tag{4}$$

of variance σ^2. The actual base-band signals leaking into the m-th receiving ADC are modeled by the convolution of a finite impulse response $h^{(m,n)}_{\mathrm{Int}}(t)$ between each individual n-th DAC output and ADC input. Assuming hardware in between the DAC output and ADC input behaves linearly, the base-band signal leaking into the m-th receiving ADC can be expressed as a superposition of all N transmitted base-band signals convolved with their respective impulse response, leading to

$$y^{(m)}_{\mathrm{Int}}(t) = \sum_{n=1}^{N} h^{(m,n)}_{\mathrm{Int}}(t) * x^{(n)}(t) \tag{5}$$

as an expression of the system's self-interference depending on its transmitted waveforms, $*$ denoting the convolution. For

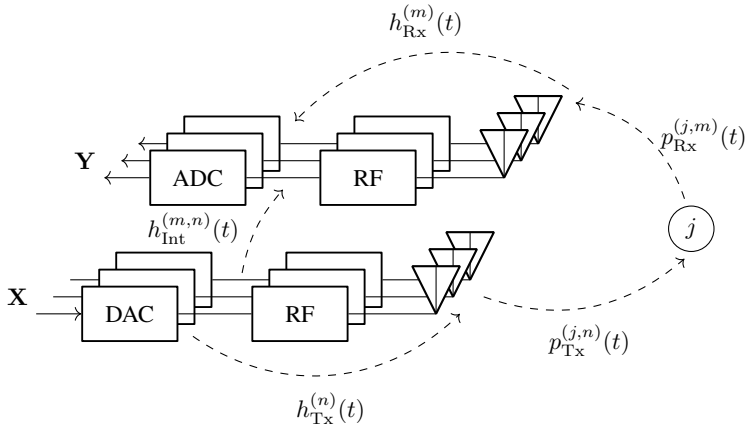

Fig. 1: System model

a single point j in the far-field of the antenna array's field of view, the waveform illuminating said point

$$z^{(j)}(t) = \sum_{\mathrm{n}=1}^{N} p_{\mathrm{Tx}}^{(j,n)}(t) * h_{\mathrm{Tx}}^{(n)}(t) * x^{(n)}(t) \tag{6}$$

can be considered a superposition of all base-band waveforms emerging from the DACs, propagated over their respective front-ends and antennas with finite impulse response $h_{\mathrm{Tx}}^{(n)}$ and traveling over the air towards the target with finite impulse response

$$p_{\mathrm{Tx}}^{(j,n)}(t) = a_{\mathrm{Tx}}^{(j,n)} \gamma_{\mathrm{Prop}}^{(j)} \delta(t - \Delta t^{(j)}) \tag{7}$$

scaled by free-space propagation loss factor $\gamma_{\mathrm{Prop}}^{(j)}$ and delayed by free-space propagation delay $\Delta t^{(j)}$. $\delta(t)$ denotes the Dirac delta function, $a_{\mathrm{Tx}}^{(j,n)}$ is the angle-of-departure dependent phase shift of a plane wave originating from the n-th transmitting antenna and impinging onto the j-th target location. Ignoring higher-order scattering by multiple subsequent targets, the signal $z^{(j)}(t)$ at location j can either be picked up by the receiving antenna of a secondary device or be scattered back to the original antenna array's receive chains scaled by a factor $\gamma_{\mathrm{Scat}}^{(j)}$. In the latter case of backscattering, the waveforms will travel back towards the m-th receiving antenna according to finite impulse response

$$p_{\mathrm{Rx}}^{(j,m)}(t) = a_{\mathrm{Rx}}^{(j,m)} \gamma_{\mathrm{Prop}}^{(j)} \delta(t - \Delta t^{(j)}) \tag{8}$$

where $a_{\mathrm{Rx}}^{(j,m)}$ represents the angle-of-arrival dependent phase shift of a plane wave originating from the j-th target location and impinging onto the m-th receiving antenna. The base-band signal resulting from environmental scattering

$$y_{\mathrm{Rad}}^{(m)}(t) = h_{\mathrm{Rx}}^{(m)}(t) * \sum_{j=1}^{J} \gamma_{\mathrm{Scat}}^{(j)} p_{\mathrm{Rx}}^{(j,m)}(t) * z^{(j)}(t) \tag{9}$$

arrives at the receiving ADCs distorted by the front-end receive finite impulse response $h_{\mathrm{Rx}}^{(m)}(t)$. The assumed overall system model is causal and finite, meaning all impulse responses

$$h(t),\ p(t) = 0 \quad \text{for} \quad t \notin \left[0, \frac{T_{\mathrm{Max}}}{4}\right] \tag{10}$$

are non-zero in only a finite window between $t = 0$ and $t = \frac{T_{\mathrm{Max}}}{4}$. Therefore, a maximum time delay T_{Max} between any transmitted waveform $\mathbf{x}(t)$ and its response in $\mathbf{y}(t)$ exists. Neglecting quantization noise, the time-discrete digital samples uploaded to the DACs can be expressed as the matrix

$$\begin{aligned}\mathbf{X} &= [\mathbf{x}(0), \mathbf{x}(T_{\mathrm{s}}), \ldots, \mathbf{x}((L-1)T_{\mathrm{s}})] \in \mathbb{C}^{N \times L} \\ &= [\mathbf{x}_1, \ldots, \mathbf{x}_N]^{\mathsf{T}}\end{aligned} \tag{11}$$

sampling the emerging base-band signals at rate $f_{\mathrm{s}} = \frac{1}{T_{\mathrm{s}}}$ in L instances. Equivalently,

$$\begin{aligned}\mathbf{Y} &= [\mathbf{y}(0), \mathbf{y}(T_{\mathrm{s}}), \ldots, \mathbf{y}((L-1)T_{\mathrm{s}})] \in \mathbb{C}^{M \times L} \\ &= [\mathbf{y}_1, \ldots, \mathbf{y}_M]^{\mathsf{T}}\end{aligned} \tag{12}$$

is the expression of L time-discrete base-band samples downloaded from the ADCs after sampling. In practice, the number of digital samples L configured for transmission and captured during reception may differ. However, for ease of notation, both sample counts will be assumed identical. Given equation (10) the system can be assumed periodic if $\mathbf{X}$ are the samples of a periodic function or $\mathbf{X}$ is zero-padded to account for the system's maximum delay with $L_{\mathrm{Pad}} > T_{\mathrm{Max}} f_{\mathrm{s}}$ zeros. Let $\mathbf{F}_L,\ \mathbf{F}_L^{-1} \in \mathbb{C}^{L \times L}$ denote the L-point discrete Fourier and inverse discrete Fourier transform matrices and $\mathscr{F}\{\cdot\}(f),\ \mathscr{F}^{-1}\{\cdot\}(t)$ denote the time-continuous Fourier and inverse Fourier transform, respectively. Then the transmitted and received sample matrices can be equivalently expressed as

$$\widetilde{\mathbf{X}} = \mathbf{X}\mathbf{F}_L = \left[\tilde{\mathbf{x}}^{(1)}, \ldots, \tilde{\mathbf{x}}^{(L)}\right] \in \mathbb{C}^{N \times L} \tag{13}$$

$$\widetilde{\mathbf{Y}} = \mathbf{Y}\mathbf{F}_L = \left[\tilde{\mathbf{y}}^{(1)}, \ldots, \tilde{\mathbf{y}}^{(L)}\right] \in \mathbb{C}^{M \times L} \tag{14}$$

in frequency domain. Given a periodic system with finite and causal impulse responses and periodic or finite $\mathbf{x}(t)$, all convolutions are cyclic and can be replaced by an element-wise scalar multiplication in discrete frequency domain. Therefore, the system model can be equivalently expressed as

$$\begin{aligned}\tilde{\mathbf{y}}^{(l)} &= \mathscr{F}\{\mathbf{y}(t)\}(l f_{\mathrm{s}}) \\ &= \tilde{\mathbf{y}}_{\mathrm{Int}}^{(l)} + \tilde{\mathbf{y}}_{\mathrm{Rad}}^{(l)} + \tilde{\mathbf{n}}^{(l)}\end{aligned} \tag{15}$$

in terms of its individual discrete frequency components for self-interference $\tilde{\mathbf{y}}_{\mathrm{Int}}^{(l)}$, environmental backscattering $\tilde{\mathbf{y}}_{\mathrm{Rad}}^{(l)}$ and noise

$$\tilde{\mathbf{n}}^{(l)} \sim \mathcal{CN}(0, \mathbf{I}_M \sigma^2) \ . \tag{16}$$

The received self-interference in the l-th frequency bin is a linear combination

$$\tilde{\mathbf{y}}_{\mathrm{Int}}^{(l)} = \widetilde{\mathbf{H}}_{\mathrm{Int}}^{(l)} \tilde{\mathbf{x}}^{(l)} \tag{17}$$

of the N frequencies transmitted in the l-th bin according to self-interference matrix

$$\begin{aligned} \widetilde{\mathbf{H}}_{\mathrm{Int}}^{(l)} &= \begin{bmatrix} \tilde{h}_{\mathrm{Int}}^{(1,1,l)} & \dots & \tilde{h}_{\mathrm{Int}}^{(1,N,l)} \\ \vdots & \ddots & \vdots \\ \tilde{h}_{\mathrm{Int}}^{(M,1,l)} & \dots & \tilde{h}_{\mathrm{Int}}^{(M,N,l)} \end{bmatrix} \in \mathbb{C}^{M \times N} \\ &= \left[\tilde{\mathbf{h}}_{\mathrm{Int}}^{(1,l)}, \dots, \tilde{\mathbf{h}}_{\mathrm{Int}}^{(N,l)} \right] \end{aligned} \tag{18}$$

carrying the individual interference weights

$$\tilde{h}_{\mathrm{Int}}^{(m,n,l)} = \mathscr{F} \left\{ h_{\mathrm{Int}}^{(m,n)}(t) \right\} (l f_{\mathrm{s}}) \tag{19}$$

between each transmitting and receiving antenna for the l-th frequency bin. The signal backscattered from the environment contained within the l-th frequency bin

$$\tilde{\mathbf{y}}_{\mathrm{Rad}}^{(l)} = \widetilde{\mathbf{H}}_{\mathrm{Rx}}^{(l)} \widetilde{\mathbf{P}}_{\mathrm{Rx}}^{(l)} \boldsymbol{\Gamma} \widetilde{\mathbf{P}}_{\mathrm{Tx}}^{(l)} \widetilde{\mathbf{H}}_{\mathrm{Tx}}^{(l)} \tilde{\mathbf{x}}^{(l)} \tag{20}$$

is masked by the receiving front ends characteristics

$$\begin{aligned} \widetilde{\mathbf{H}}_{\mathrm{Rx}}^{(l)} &= \mathscr{D} \left\{ \tilde{h}_{\mathrm{Rx}}^{(1,l)}, \dots, \tilde{h}_{\mathrm{Rx}}^{(M,l)} \right\} \in \mathbb{C}^{M \times M} \\ \tilde{h}_{\mathrm{Rx}}^{(m,l)} &= \mathscr{F} \left\{ h_{\mathrm{Rx}}^{(m)}(t) \right\} (l f_{\mathrm{s}}) \end{aligned} \tag{21}$$

within the respective frequency bins during reception and depends on the transmitted frequencies masked by the transmitting front end characteristics

$$\begin{aligned} \widetilde{\mathbf{H}}_{\mathrm{Tx}}^{(l)} &= \mathscr{D} \left\{ \tilde{h}_{\mathrm{Tx}}^{(1,l)}, \dots, \tilde{h}_{\mathrm{Tx}}^{(N,l)} \right\} \in \mathbb{C}^{N \times N} \\ \tilde{h}_{\mathrm{Tx}}^{(n,l)} &= \mathscr{F} \left\{ h_{\mathrm{Tx}}^{(n)}(t) \right\} (l f_{\mathrm{s}}) \ . \end{aligned} \tag{22}$$

III. Self-Interference Estimation

In a controlled environment, where it can be ensured that no target is in the antenna array's field of view, meaning the number of targets $J = 0$, the system model

$$\tilde{\mathbf{y}}^{(l)} \Big|_{J=0} = \widetilde{\mathbf{H}}_{\mathrm{Int}}^{(l)} \tilde{\mathbf{x}}^{(l)} + \tilde{\mathbf{n}}^{(l)} \tag{23}$$

simplifies to only self-interference and noise by dropping the environmental scattering term. Since the antenna array is fully digital, there is full control over the base-band waveform transmitted over each RF chain at any point in time. This can be exploited to estimate the array's self-interference characteristics by transmitting a sequence of O probing waveforms

$$\begin{aligned} \widetilde{\mathbf{X}}_{\mathrm{Cal}}^{(n,o)} &= \left[\tilde{\mathbf{x}}_{\mathrm{Cal}}^{(1,n,o)}, \dots, \tilde{\mathbf{x}}_{\mathrm{Cal}}^{(N,n,o)} \right]^{\mathsf{T}} \\ &= \left[\tilde{\mathbf{x}}_{\mathrm{Freq}}^{(n,1,o)}, \dots, \tilde{\mathbf{x}}_{\mathrm{Freq}}^{(n,L,o)} \right] \end{aligned} \in \mathbb{C}^{N \times L} \tag{24}$$

W over all N DACs sequentially, so that during transmission over the n-th DAC

$$\tilde{\mathbf{x}}_{\mathrm{Cal}}^{(n',n,o)} = \begin{cases} \tilde{\mathbf{u}}_{\mathrm{Cal}}^{(o)} & \text{for } n' = n \\ \mathbf{0} & \text{otherwise} \end{cases} \tag{25}$$

the remaining $N - 1$ DACs are muted and the n-th DAC transmits probing waveform $\tilde{\mathbf{u}}_{\mathrm{Cal}}^{(o)}$. Let

$$\begin{aligned} \widetilde{\mathbf{U}} &= \left[\tilde{\mathbf{u}}_{\mathrm{Cal}}^{(1)}, \dots, \tilde{\mathbf{u}}_{\mathrm{Cal}}^{(O)} \right]^{\mathsf{T}} \\ &= \left[\tilde{\mathbf{u}}_{\mathrm{Freq}}^{(1)}, \dots, \tilde{\mathbf{u}}_{\mathrm{Freq}}^{(L)} \right] \end{aligned} \in \mathbb{C}^{O \times L} \tag{26}$$

be the matrix consisting of all O probing waveforms in frequency domain, so that

$$\tilde{\mathbf{u}}_{\mathrm{Freq}}^{(l)} = \left[\tilde{u}^{(l,1)}, \dots, \tilde{u}^{(l,O)} \right]^{\mathsf{T}} \in \mathbb{C}^{O} \tag{27}$$

is the vectorization of the l-th frequency bin of all O probing waveforms stacked. The frequency-domain samples

$$\widetilde{\mathbf{Y}}_{\mathrm{Cal}}^{(n,o)} = \left[\tilde{\mathbf{y}}_{\mathrm{Cal}}^{(n,1,o)}, \dots, \tilde{\mathbf{y}}_{\mathrm{Cal}}^{(n,L,o)} \right] \in \mathbb{C}^{M \times L} \tag{28}$$

received during the o-th probing of the n-th transmitting DAC

$$\tilde{\mathbf{y}}_{\mathrm{Cal}}^{(n,l,o)} = \left[\tilde{y}_{\mathrm{Cal}}^{(1,n,l,o)}, \dots, \tilde{y}_{\mathrm{Cal}}^{(M,n,l,1)} \right] \tag{29}$$

$$= \widetilde{\mathbf{H}}_{\mathrm{Int}}^{(l)} \tilde{\mathbf{x}}_{\mathrm{Freq}}^{(n,l,o)} + \tilde{\mathbf{n}}^{(n,l,o)} \tag{30}$$

$$= \tilde{\mathbf{h}}_{\mathrm{Int}}^{(n,l)} \tilde{u}^{(l,o)} + \tilde{\mathbf{n}}^{(n,l,o)} \tag{31}$$

depend on the self interference weights between the DAC output and all receiving ADCs $\tilde{\mathbf{h}}_{\mathrm{Int}}^{(n,l)}$ scaled by the l-th frequency bin of the o-th probing wavefeorm $\tilde{u}^{(l,o)}$. The vectorization of the obtained samples for a single frequency bin

$$\begin{aligned} \tilde{\mathbf{v}}^{(m,n,l)} &= \left[\tilde{y}_{\mathrm{Cal}}^{(m,n,l,1)}, \dots, \tilde{y}_{\mathrm{Cal}}^{(m,n,l,O)} \right]^{\mathsf{T}} \\ &= \tilde{h}^{(m,n,l)} \tilde{\mathbf{u}}_{\mathrm{Freq}}^{(l)} + \tilde{\mathbf{n}}^{(m,n,l)} \end{aligned} \tag{32}$$

is in turn dependent on only the scalar self-interference frequency bin weight $\tilde{h}^{(m,n,l)}$ and a circularly invariant additive Gaussian noise component of variance σ^2. Then, the antenna array's frequency-domain self-interference characteristics

$$\widehat{\mathbf{H}}_{\mathrm{Int}}^{(l)} = \begin{bmatrix} \hat{h}_{\mathrm{Int}}^{(1,1,l)} & \dots & \hat{h}_{\mathrm{Int}}^{(1,N,l)} \\ \vdots & \ddots & \vdots \\ \hat{h}_{\mathrm{Int}}^{(M,1,l)} & \dots & \hat{h}_{\mathrm{Int}}^{(M,N,l)} \end{bmatrix} \in \mathbb{C}^{M \times N} \tag{33}$$

can be estimated independently for all L frequency bins by computing the scalar minimum mean-square error estimates [10]

$$\hat{h}_{\mathrm{Int}}^{(m,n,l)} = \tilde{\mathbf{u}}_{\mathrm{Freq}}^{(l)\mathsf{H}} \left(\tilde{\mathbf{u}}_{\mathrm{Freq}}^{(l)} \tilde{\mathbf{u}}_{\mathrm{Freq}}^{(l)\mathsf{H}} + \sigma^2 \mathbf{I}_O \right)^{-1} \tilde{\mathbf{v}}_{\mathrm{Cal}}^{(m,n,l)} \tag{34}$$

for each pair of transmit and receive chains.

IV. Precoding

The antenna array's transmitting elements should illuminate the j-th target location with an expected arbitrary communication waveform, represented by frequency bins

$$\tilde{\mathbf{w}} = \left[\tilde{w}^{(1)}, \dots, \tilde{w}^{(L)}\right]^{\intercal} \in \mathbb{C}^{L} \ , \tag{35}$$

while simultaneously minimizing their self-interference by precoding the expected waveform with

$$\widetilde{\mathbf{C}} = \left[\tilde{\mathbf{c}}^{(1)}, \dots, \tilde{\mathbf{c}}^{(L)}\right] \in \mathbb{C}^{N \times L} \tag{36}$$

so that the actually transmitted waveform over all DACs is

$$\widetilde{\mathbf{X}}_{\mathrm{Pre}} = \widetilde{\mathbf{C}} \, \mathscr{D}\left\{\mathbf{w}\right\} \ . \tag{37}$$

Given that an estimate of the antenna array's self-interference characteristics $\widehat{\mathbf{H}}_{\mathrm{Int}}^{(l)}$ is available, finding such a precoding can be formulated as a constrained optimization problem

$$\begin{aligned} \min_{\tilde{\mathbf{c}}^{(l)} \in \mathbb{C}^{N}} \quad & \frac{1}{2} \| \widehat{\mathbf{H}}_{\mathrm{Int}}^{(l)} \tilde{\mathbf{c}}^{(l)} w^{(l)} \|_2^2 \\ \text{s.t.} \quad & \mathbf{a}^{\intercal} \tilde{\mathbf{c}}^{(l)} = 1 \\ & \| \tilde{c}^{(n,l)} w^{(l)} \| \leq \| w^{(l)} \| \quad \forall \ n = 1 \dots N \end{aligned} \tag{38}$$

that can be solved independently for each individual frequency bin. The equality constraint $\mathbf{a}^{\intercal} \tilde{\mathbf{c}}^{(l)} = 1$ ensures that the transmitted power is focused towards the desired target location by considering the antenna array's far-field phase response $\mathbf{a}$ towards the target's direction. The objective has multiple solutions, which can be understood by considering that for two transmitting antennas, the signals that cancel each other out at a single receiving antenna can be any combination of amplitudes, as long as the respective phases match. However, the transmitting DACs have limited dynamic range, so that a high difference in overall signal amplitudes will lead to a decrease in transmitted power. In order to avoid highly dynamic solutions, the absolute amplitude of all frequency precoding bins is limited to one, represented by the inequality constraint $\| \tilde{c}^{(n,l)} \| \leq 1$. A problem of the above form has the relaxed closed-form dual solution

$$\tilde{\mathbf{c}}^{(l)} = \frac{\left(\widehat{\mathbf{H}}_{\mathrm{Int}}^{(l)\mathsf{H}} \widehat{\mathbf{H}}_{\mathrm{Int}}^{(l)} + \lambda \mathbf{I}_N \right)^{-1} \mathbf{a}}{\mathbf{a}^{\intercal} \left(\widehat{\mathbf{H}}_{\mathrm{Int}}^{(l)\mathsf{H}} \widehat{\mathbf{H}}_{\mathrm{Int}}^{(l)} + \lambda \mathbf{I}_N \right)^{-1} \mathbf{a}} \tag{39}$$

with regularization parameter $\lambda \in \mathbb{R}_{+}$. Curiously, for $\lambda = 0$, this solution coincides with the minimum variance distortionless beamformer proposed in [11], only that instead of minimizing the interference with other devices the antenna array's internal self-interference is minimized.

V. Validation

Both the proposed self-interference estimation approach in section III and the proposed self-interference cancellation approach in section IV were implemented in a Software Defined Radio (SDR) setup as an extension of the Heterogeneous Mobile Radio Simulator Python (HermesPy) [12]. The respective Python source code, including instructions to reproduce all measurements and generated graphs, is publicly available on GitHub [13]. The validation hardware consists of two synchronized Ettus x410 SDR units [14] operating at 6 GHz carrier frequency with 490 MHz bandwidth, one unit receiving over a single horn antenna representing a communication terminal and one unit featuring an array of five horn antennas, two antennas of which are connected to receiving ports and three to transmitting ports, representing a base station jointly communicating with the terminal and detecting objects in its field of view by picking up back-scattered power over its single receiving antenna. Figure 2 displays the considered setup, with

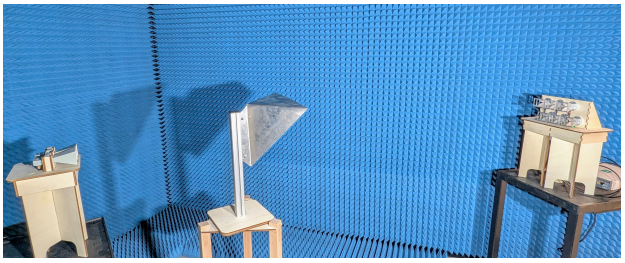

Fig. 2: Software defined radio measurement setup

the communication receiver to the left and the base station to the right. In between the two, at approximately 1.5 m, a corner reflector facing the base station represents a target to be detected. The self-interference estimation performance is assessed by comparing the root-mean square error

$$\mathrm{RMSE} = \sqrt{\frac{1}{ML} \sum_{l=1}^{L} \| \widehat{\mathbf{H}}^{(l)} \tilde{\mathbf{x}}^{(l)} - \tilde{\mathbf{y}}^{(l)} \|_2^2} \tag{40}$$

between the leaking signal predicted by the self-interference estimation when transmitting a random white-noise signal over all transmitting antennas in a target-free environment and the actually measured leaking signal. Different noise powers are achieved by varying the SDR's receive gain in the available range from 0 dB to 60 dB. The respective noise power

$$\hat{\sigma}^2 = \frac{1}{ML} \sum_{m=1}^{M} \| \mathbf{y}_m \|_2^2 \ \Bigg|_{\mathbf{X}=\mathbf{0}} \tag{41}$$

for each receive gain candidate is estimated by averaging the device's received samples without any configured transmissions, meaning $\mathbf{X} = \widetilde{\mathbf{X}} = \mathbf{0}$. The results are visualized in Figure 3. The self-interference mitigation performance of the proposed precoding is assessed by observing the difference in the transmitted power and the power leaking into the receive chains of an Orthogonal Frequency Division Multiplexing (OFDM) waveform, featuring a Schmidl-Cox pilot section and a single symbol section consisting of 256 quadrature-amplitude modulated symbols, for different values of the regularization parameter λ. OFDM was selected as a validation waveform due to its widespread adoption in current communication standards, however, the proposed precoding is not limited to OFDM and applicable to virtually any sequence of base-band samples. The precoding's effect on power leaking from the base station's transmitting DACs into its receiving

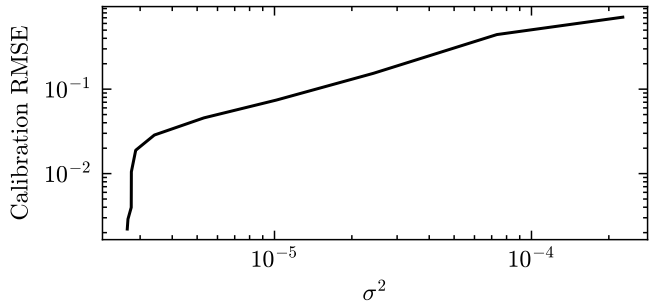

Fig. 3: Calibration performance

ADCs is visualized in Figure 4. As expected, the smaller λ is

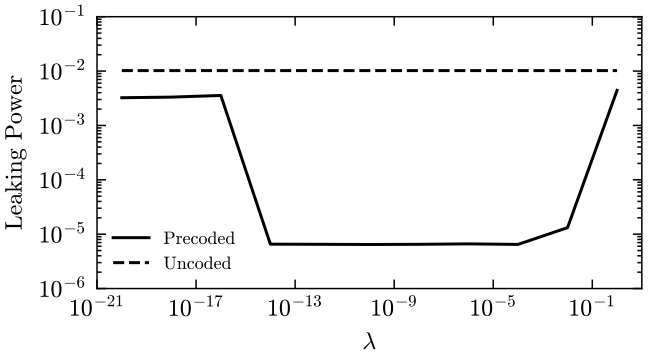

Fig. 4: Precoding performance

chosen, the bigger the leakage suppression, with a maximum leakage difference of 30 dB compared to a conventionally beamformed signal labeled "Uncoded" around $\lambda = 10^{-10}$. For regularization values smaller than $\lambda = 10^{-14}$ a rise in leaking power to levels above $\lambda = 10^{-1}$ is observable, leading to a region of high leakage suppression located roughly in between the two limits. The precoding's effect on the power received by the communication terminal is visualized in Figure 5. Compared to the "Uncoded" signal, the proposed precoding

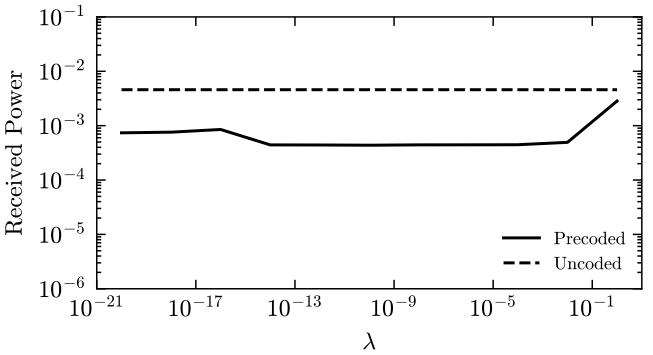

Fig. 5: Received communication power

loses approximately 10 dB of received power in the region of high leakage suppression. Therefore, the gain of the proposed precoding scheme in this specific hardware setup can be considered to be approximately 20 dB. Within the conducted measurement campaign, there was no observable difference in communication performance for regularization values greater than $\lambda = 10^{-14}$, as shown by the Error Vector Magnitude (EVM) depicted in Figure 6. After precoding, the remaining

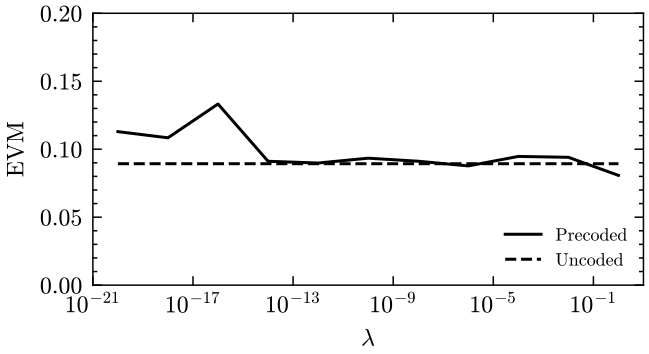

Fig. 6: Communication performance

signal components sampled by the base station's receiving ADCs can be considered scattering from the environment and can be exploited to detect objects in the base station antenna array's field of view by a matched-filter approach convolving the expected reception with the actually received samples and deriving a range-power profile from the results [15]. Figure 7 depicts the mean power over range bin estimates for 400 consecutive OFDM frames, comparing a conventionally beamformed signal with the proposed precoded approach at $\lambda = 10^{-10}$. For both waveforms, two graphs are visualized,

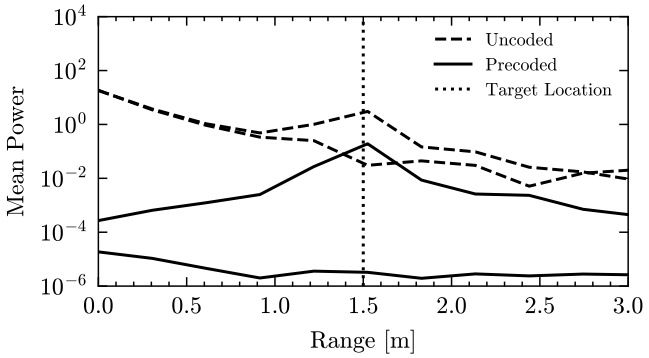

Fig. 7: Radar range-power profile

with the graph lower in power at 1.5 m representing an empty field of view and the graph higher in power at 1.5 m representing a placed corner reflector. While the conventional approach is higher in overall received power, the proposed precoding rejects the majority of the leaking power around the zero range bin. Additionally, compared to the conventional approach, the difference in power between an empty field of view and an existing target significantly improves. Considering a simple threshold detector assuming a target at the maximum power range bin, the improved leakage rejection enables an almost perfect detection performance at $\lambda = 10^{-10}$, as indicated by the receiver operating characteristics depicted in Figure 8.

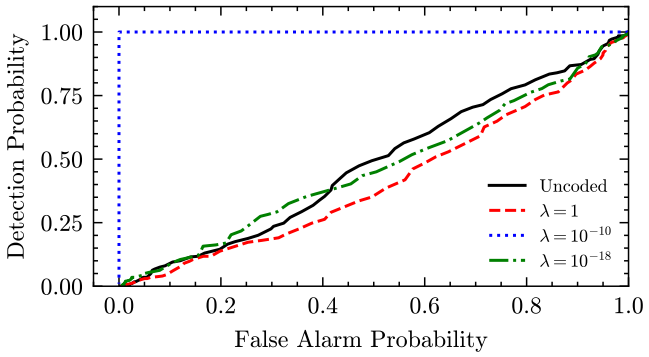

Fig. 8: Detection performance

VI. Conclusion

In this work, the problem of digitally estimating and mitigating self-interference in fully digital sensing and communication multi-antenna arrays was introduced. It could be shown, both theoretically and in an experimental setup, that self-interference in between the transmitting and receiving analog RF chains of antenna arrays featuring a dedicated DAC or ADC for each individual antenna can be decreased by digitally precoding waveforms emerging from the DACs, given that a good estimate of the self-interference characteristics is available. While these findings serve as a motivation for further investigations, some shortcomings should be addressed in the future:

- The system model assumes ideal RF front-ends with perfect linearity, accounting for non-linearities might greatly improve the overall performance.
- The proposed calibration algorithm requires an initial empty field of view, which is only feasible under controlled laboratory conditions.
- The precoding's effect on the overall beamforming characteristics and peak-to-average power ratio is unclear.

References

[1] A. Bourdoux, A. N. Barreto, B. van Liempd, C. d. Lima, D. Dardari, D. Belot, E.-S. Lohan, G. Seco-Granados, H. Sarieddeen, H. Wymeersch, J. Suutala, J. Saloranta, M. Guillaud, M. Isomursu, M. Valkama, M. R. K. Aziz, R. Berkvens, T. Sanguanpuak, T. Svensson, and Y. Miao, "6G White Paper on Localization and Sensing." [Online]. Available: http://arxiv.org/pdf/2006.01779v1

[2] T. Wild, V. Braun, and H. Viswanathan, "Joint Design of Communication and Sensing for Beyond 5G and 6G Systems," *IEEE Access*, vol. 9, pp. 30 845–30 857, 2021.

[3] H. Tataria, M. Shafi, A. F. Molisch, M. Dohler, H. Sjoland, and F. Tufvesson, "6G Wireless Systems: Vision, Requirements, Challenges, Insights, and Opportunities," *Proceedings of the IEEE*, vol. 109, no. 7, pp. 1166–1199, 2021.

[4] Z. Wei, F. Liu, C. Masouros, N. Su, and A. P. Petropulu, "Toward Multi-Functional 6G Wireless Networks: Integrating Sensing, Communication, and Security," *IEEE Communications Magazine*, vol. 60, no. 4, pp. 65–71, 2022.

[5] F. Liu, Y. Cui, C. Masouros, J. Xu, T. X. Han, Y. C. Eldar, and S. Buzzi, "Integrated Sensing and Communications: Toward Dual-Functional Wireless Networks for 6G and Beyond," *IEEE Journal on Selected Areas in Communications*, vol. 40, no. 6, pp. 1728–1767, 2022.

[6] F. Bozorgi, P. Sen, A. N. Barreto, and G. Fettweis, "RF Front-End Challenges for Joint Communication and Radar Sensing," in *2021 1st IEEE International Online Symposium on Joint Communications & Sensing (JC&S)*. IEEE, 2021, pp. 1–6.

[7] A. Sabharwal, P. Schniter, D. Guo, D. W. Bliss, S. Rangarajan, and R. Wichman, "In-band full-duplex wireless: Challenges and opportunities," *IEEE Journal on Selected Areas in Communications*, vol. 32, no. 9, pp. 1637–1652, 2014.

[8] S. Hong, J. Brand, J. I. Choi, M. Jain, J. Mehlman, S. Katti, and P. Levis, "Applications of self-interference cancellation in 5g and beyond," *IEEE Communications Magazine*, vol. 52, no. 2, pp. 114–121, 2014.

[9] J. Zhang, F. He, W. Li, Y. Li, Q. Wang, S. Ge, J. Xing, H. Liu, Y. Li, and J. Meng, "Self-interference cancellation: A comprehensive review from circuits and fields perspectives," *Electronics*, vol. 11, no. 2, 2022.

[10] H. Yin, D. Gesbert, M. Filippou, and Y. Liu, "A coordinated approach to channel estimation in large-scale multiple-antenna systems," *IEEE Journal on Selected Areas in Communications*, vol. 31, no. 2, pp. 264–273, 2013.

[11] O. Frost, "An algorithm for linearly constrained adaptive array processing," *Proceedings of the IEEE*, vol. 60, no. 8, pp. 926–935, 1972.

[12] J. Adler, T. Kronauer, and A. N. Barreto, "HermesPy: An Open-Source Link-Level Evaluator for 6G," *IEEE Access*, vol. 10, pp. 120 256–120 273, 2022.

[13] J. Adler, "Self interference cancellation source code," https://github.com/adlerjan/mimo-sic-jcns-2025, 2025.

[14] NI, "Ettus USRP X410 Specifications," 2024-03-22. [Online]. Available: https://www.ni.com/docs/en-US/bundle/ettus-usrp-x410-specs/page/specs.html

[15] J. Adler, J. Kugelmann, M. Matthé, and P. Sen, "Demonstration of Joint Communication and Sensing with Fully Digital Arrays," in *2025 5th IEEE International Symposium on Joint Communications & Sensing (JC&S)*, 2025, to appear.